Physico-chemical insights into gas-phase and oxide-supported sub-nanometre AuCu clusters

Hussein, Heider; Gao, Mansi; Hou, Yiyun; Horswell, Sarah L; Johnston, Roy

DOI:
10.1515/zpch-2018-1356

Heider A. Hussein, Mansi Gao, Yiyun Hou, Sarah L. Horswell, and Roy L. Johnston*

Physico-chemical insights into gas-phase and oxide-supported sub-nanometre AuCu clusters

Abstract: Catalysis by AuCu nanoclusters is a promising scientific field. However, our fundamental understanding of the underlying mechanisms of mixing in AuCu clusters at the sub-nanometre scale and their physico-chemical properties in both the gas-phase and on oxide supports is limited. We have identified the global minima of gas-phase and MgO(100)-supported AuCu clusters with 3-10 atoms using the Mexican Enhanced Genetic Algorithm coupled with density functional theory. Au and Cu adatoms and supported dimers have been also simulated at the same level of theory. The most stable composition, as calculated from mixing and binding energies, is obtained when the Cu proportion is close to 50%. The structures of the most stable free AuCu clusters exhibit Cu-core/Au-shell segregation. On the MgO surface however, there is a preference for Cu atoms to lie at the cluster-substrate interface. Due to the interplay between the number of interfacial Cu atoms and surface-induced cluster rearrangement, on the MgO surface 3D structures become more stable than 2D structures. The O-site of MgO surface is found to be the most favourable adsorption site for both metals. All dimers favour vertical (V) configurations on the surface and their adsorption energies are in the order: **Au**Cu < Cu**Cu** < Au**Au** < Au**Cu** (where the bold atom is bound to the O-site). For both adatoms and AuCu dimers, adsorption via Cu is more favourable than Au- adsorbed configurations, but, this disagrees with the ordering for the pure dimers due to a combination of electron transfer and the metal-on-top effect. Binding energy (and second difference) and HOMO-LUMO gap calculations show that even-atom (even-electron) clusters are more stable than the neighbouring odd-atom (odd-electron) clusters, which is expected for closed- and open-shell systems. Supporting AuCu clusters on the MgO(100) surface decreases the charge transfer between Au and Cu atoms calculated in free clusters. The results of this study may serve as a foundation for designing better AuCu catalysts.

Keywords: Genetic Algorithm, Global Optimisation, AuCu clusters, oxide-supported clusters.

Heider A. Hussein, Mansi Gao, Yiyun Hou, Sarah L. Horswell, Roy L. Johnston, School of Chemistry, University of Birmingham, Birmingham, B15 2TT, United Kingdom; Email: r.l.johnston@bham.ac.uk

Heider A. Hussein, Department of Chemistry, College of Science, University of Kufa, Najaf, Iraq

1 Introduction

Promising technological applications of oxide-supported nanoparticles, including high density computer memory and highly active and selective catalysts, have attracted great research interest over recent years and have driven research to understand the metal/metal-oxide interface [1]. Improved knowledge of the interactions between metal clusters and oxide supports are essential for the design of new, improved catalysts. The unusual catalytic properties of nanoparticles, not seen in their corresponding bulk counterparts, can be highly affected by the choice of support [2]. The effect of the surface on the metal cluster/nanoparticle catalyst can be due to electronic effects (e.g. modification of the metal oxidation states and/or the density of electronic states) or geometric effects (e.g. due to lattice-mismatch-induced strain) [3] .

When clusters are deposited on an oxide support, nanoparticle growth may occur, leading to fewer, but larger nanoparticles and lowering the total active surface for a given mass (and, therefore, increasing the cost) of metal [3, 4]. An important goal is, therefore, to control the size and distribution of the nanoparticles by controlling the individual steps of adsorption, diffusion, nucleation and sintering [4, 5]. Because of the widespread experimental use of the MgO(100) surface [6, 7] as an inert support [8] and the simplicity of its structure [6, 9–13], the MgO(100) surface has been studied extensively. In the field of nanoclusters, however, fascinating technological applications of MgO(100)- supported clusters have attracted increasing attention, but knowledge of "surface magic clusters" is lacking compared to that of gas-phase "magic clusters" [9] .

It is well known that doping (or alloying) a one metal into a cluster of another metal can effectively change its electromagnetic and structural properties, which can be used to tune the physico-chemical properties of the cluster [14–20]. The electronic shell model is the main approach that can be used to explain the enhanced stability for specific sizes of such systems [19] . In recent work, we have demonstrated that $Pd_1Au_6^+$ has a different structure (a Pd-capped Au_6 triangle) to the pure Au_7^+ cluster (a centred hexagon), which is also related to its anomalously high stability to photofragmentation [14]. Although the Pd-doped cluster has an odd number of electrons, it has high stability because the Pd atom donates one electron towards the planar Au_6 triangular fragment, resulting in 6 delocalised cluster electrons, which is a magic number for a 2D cluster. The sigma aromaticity in the Au_5Zn^+ cluster has also been found to enhance its stability [21]. Doping a single Mo, W, Zr or Hf atom into Au_{12} and Au_{14} clusters was found to lead to an increase in the energy gap between the highest occupied molecular orbital (HOMO) and the lowest unoccupied molecular orbital (LUMO) [17, 22], leading to enhanced cluster stability [20].

Copper clusters at the nanoscale have received significant attention recently due to their potential as catalysts in environmental applications [23, 24]. These clusters have the ability to catalyse a wide variety of chemical reactions, including CO_2 reduction and

CO oxidation [25–27]. The only drawback for the practical applications of Cu clusters as catalysts is its facile oxidation to form CuO and Cu_2O [28, 29] and it is well known that the oxidation of copper can compromise its catalytic activity, leading to a decrease of the catalyst lifetime in oxidative environments. Stabilizing the Cu catalyst by alloying with different elements, however, can increase its resistance to oxidation [30–32]. Considerable interest has, therefore, been focused on CuAu nanoclusters, due to their higher resistance to oxidation and corrosion [25, 26, 33]. Although the crystal structures of bulk Cu and Au and their ordered intermetallic phases are the same (ccp) [34], the physico-chemical properties of Cu and Au are significantly different [19, 35]. In addition to improving the catalytic properties, inclusion of Cu atoms as additives to noble metallic clusters, including Au clusters, also decreases the cost of the catalysts [36–38]. AuCu nanoalloys have been proven previously to be promising catalysts for propene epoxidation, CO oxidation and benzyl alcohol oxidation [39–41]. Both Au@Cu and Cu@Au core-shell clusters have been prepared with well-controlled sizes and characterized by electron microscopy [42]. Theoretical researches have shown that a Cu-rich core/Au-rich shell is the lowest energy chemical ordering at equilibrium [43–45]. Other research showed that exposing Au-rich core/Cu-rich shell particles leads to rapid surface oxidation in air, while the Cu-rich core/Au-rich shell configuration is stable to oxidation [46].

The interactions between AuCu nanoclusters and an oxide surface can lead to rearrangements in both the chemical ordering and the geometric structure of the cluster. It has reported that the fcc truncated octahedron is found to be the optimal morphology on the surface when depositing AuCu nanoclusters on the MgO substrate [43]. An fcc structure is found to be the predominant motif for MgO-supported AuCu nanoclusters that have the following stoichiometric compositions: Au:Cu = 0.25:0.75, 0.5:0.5, and 0.75:0.25, suggesting a cube-on-cube orientation with the MgO(100) substrate [43]. The 0.5:0.5 composition AuCu catalyst deposited on MgO powder showed much greater activity than the corresponding Cu-rich or Au-rich clusters for the catalytic reduction of 4-nitrophenol at room temperature [37]. Due to the synergistic interaction between Cu and Au atoms, AuCu catalysts exhibit increased activity for low temperature CO oxidation and higher resistance to sintering compared with the pure clusters [47, 48]. Mozer et al. [49] reported that high copper content in AuCu clusters can block the Au active sites, thus Cu-deficient clusters have increased catalytic activity for CO oxidation. Research of Ma and co-workers [8, 50] on AuCu clusters on MgO showed that $Au_{15}Cu_{15}$ on MgO(100) has high activity for the dissociation of O_2.

Studying sub-nanometre AuCu clusters, where quantum effects are observed and where “every atom counts” [51, 52], is required in order to rationalize their catalytic activity and to form a base for future experimental investigations. To the best of our knowledge, detailed, systematic studies of MgO-supported sub-nanometre AuCu clusters have not been reported, despite many publications on the structural and catalytic properties of larger free and MgO-supported AuCu nanoparticles [8, 50, 53-

55]. Theoretically, sub-nanometre sizes present a synergistic combination between employing high level theory (e.g. Density Functional Theory, DFT), required to study quantum size effects, with direct global optimisation [56]. Motivated by our previous successful genetic algorithm (GA) [57] application to 8-atom AuCu sub-nanometre clusters [35, 58], we employ here the Mexican Enhanced Genetic Algorithm (MEGA) [56, 59] coupled with DFT to present a comprehensive prediction of physico-chemical properties for all compositions of binary sub-nanometre AuCu clusters in the size range 3-10 atoms, including a comparison with the pure metal clusters and MgO(100)-supported clusters. Calculations on supported adatoms and dimers are also included for comparison.

2 Methodology

The MEGA global optimisation program [59] was applied at the DFT level to investigate the lowest energy structures of Au-Cu sub-nanometre clusters both in the gas-phase and supported on the MgO(100) surface. The putative global minima (GM) for our studied system in the size range 3-10 atoms were calculated for all compositions, starting from randomly-generated structures, which were subsequently locally minimised at the DFT level. Similar to our previous GA version, the Birmingham Parallel Genetic Algorithm (BPGA) [60], MEGA employs a pool methodology for the parallel evaluation of structures [61, 62]. The initial pool is formed from ten generated isomers which are geometrically relaxed locally by DFT energy minimization. Members of the minimized structures are selected then for either crossover or mutation operations. For crossover operation, pairs of the clusters are selected using the tournament selection method, based on a fitness criterion. The cut-and-splice method introduced by Deaven and Ho [63] is used to form offspring clusters. Four mutation operations can be applied for randomly selected clusters: “move,” “rotate,” “twist,” and “atom inversion”. The mutation operation produces 20% of the new clusters in the population and the rest are generated by the crossover operation. Further details of the MEGA code are given in Refs [56, 59].

Gamma-point DFT calculations were performed using the Vienna Ab-initio Simulation Package (VASP) [64]. The calculations utilised Projected Augmented Wave (PAW) pseudopotentials and the Perdew-Burk-Erzenhof (PBE) generalized gradient approximation exchange correlation functional [65, 66] with an energy cut-off of 400 eV. Convergence was improved by implementing Methfessel-Paxton smearing [67], with a sigma value of 0.01 eV. A plane-wave basis set was used, including spin polarization. The thresholds for the electronic energy and forces were set to 10^{-6} eV and 10^{-5} eV/Å, respectively. Frequency analysis was performed to ensure that the structures obtained are true minima on the DFT energy surface.

In the search for the GM of the supported clusters, the cluster geometries were

relaxed within a sphere placed 1.5 Å above a frozen 2-layer MgO(100) slab. A 6x6x2 slab was used for clusters with N < 8 atoms and an 8x8x2 slab for N ≥ 8 atoms. These slab sizes were chosen to prevent unphysical cluster-cluster interactions and a vacuum spacing of 14.7 Å was used.

Adatom and supported dimer systems were built manually and minimized directly (at the DFT level), without needing to use the GA. For the deposition of monomers on the (100) surface, we employed four different initial configurations for a single Au or Cu atom on the surface: the on-top oxygen site (O), the on-top magnesium site (Mg), the Mg-O bridge site, and the fourfold hollow site (H). For the deposition of dimers (Au-Au, Cu-Cu, and Au-Cu), two possible initial orientations of the dimer, with respect to the surface, were investigated: perpendicular or vertical (V), and parallel (P). For the homonuclear dimers, Au_2 and Cu_2, the V orientation gives rise to 4 configurations, corresponding to the same sites as for adatoms, as shown in Figure (1). However, for the AuCu dimer, there are 8 starting configurations, as either the Au or the Cu atom can be closest to the surface. For the P orientation, as shown in Figure (2), 10 starting configurations were considered for the AuCu dimer, while there are only 9 inequivalent P configurations for Au_2 and Cu_2, as configuration 10 is equivalent to configuration 4 for the homonuclear diatomics.

Ionization energies (I) and electron affinities (A) were calculated for all free and supported clusters, using Koopman's approximation [68]:

$$I = -E_{HOMO} \qquad (1)$$
$$A = -E_{LUMO} \qquad (2)$$

I and A were subsequently used to calculate the conceptual DFT-based descriptors: electronegativity (χ), global hardness (η), molecular softness (S), and electrophilicity index (ω), which are given by:

$$\chi = -\mu = \frac{I + A}{2} \qquad (3)$$

where μ represents the chemical potential of the system.

$$\eta = \frac{I - A}{2} \qquad (4)$$
$$S = \frac{1}{2\eta} \qquad (5)$$
$$\omega = \frac{\mu^2}{2\eta} \qquad (6)$$

For free and supported pure and mono-substituted Au and Cu clusters, the stability

of each cluster, relative to neighbouring sizes, is indicated by the second difference in energy ($\Delta_2 E$):

$$\Delta_2 E = E(A_{N+1}) + E(A_{N-1}) - 2E(A_N) \qquad (7)$$

where $E(A_N)$ corresponds to the energy of the N-atom cluster and $E(A_{N+1})$ and $E(A_{N-1})$ are the energies of the neighbouring clusters.

The effect of doping Au atoms into Cu clusters was evaluated by calculating the mixing energy (Δ):

$$\Delta = E_{(Au_m Cu_n)} - m\frac{E_{(Au_N)}}{N} - n\frac{E_{(Cu_N)}}{N} \qquad (8)$$

where $E_{(Au_m Cu_n)}$ is the total energy of the cluster $Au_m Cu_n$, m and n are the numbers of Au and Cu atoms, respectively, and $E_{(Au_N)}$ and $E_{(Cu_N)}$ are the energies of the pure Au and Cu clusters of the same size ($N = m + n$), respectively.

The average binding energy per atom (E_b) is given by:

$$E_b = -\frac{1}{N}\left[E_{(Au_m Cu_n)} - m\,E_{(Au)} - n\,E_{(Cu)}\right] \qquad (9)$$

where $E_{(Au)}$ and $E_{(Cu)}$ are the electronic energies of single Au and Cu atoms, respectively.

The adsorption energy, E_{ads}, for a supported cluster is calculated as:

$$E_{ads} = E_{(slab+Au_m Cu_n)} - E_{(slab)} - E_{(Au_m Cu_n)} \qquad (10)$$

where $E_{(slab+Au_m Cu_n)}$ is the total energy of the supported cluster/slab system, $E_{(slab)}$ is the energy of the surface slab, and $E_{(Au_m Cu_n)}$ is the energy of the free $Au_m Cu_n$ cluster, locally minimized in the gas phase.

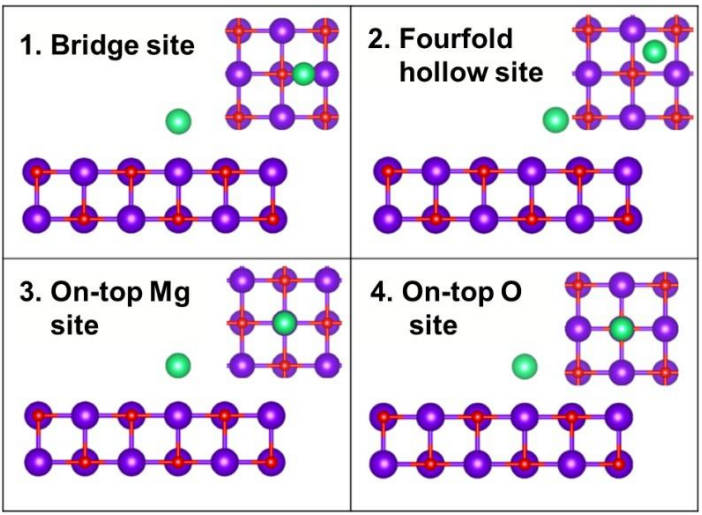

Fig. 1: The starting positions for adatoms and V configurations of supported dimers. Mg and O atoms are shown (here, and in subsequent figures) in purple and red, respectively, while the green spheres represent the starting position of the adatom or the lower atom of the dimer.

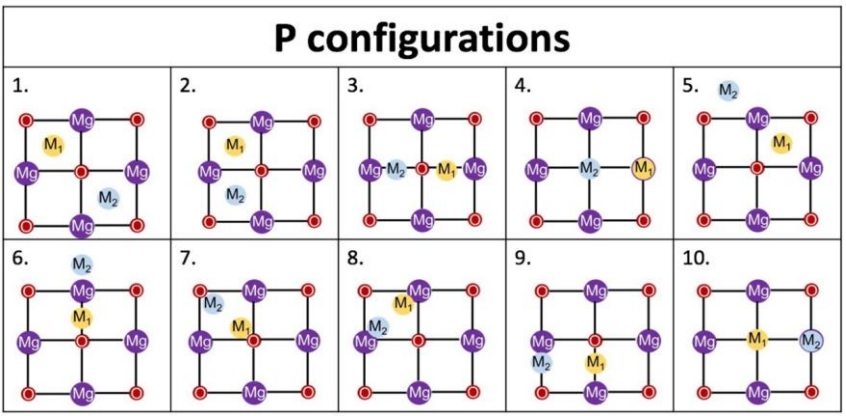

Fig. 2: Schematic representation of starting positions for P configurations of supported dimers. Au and Cu atoms are represented by M1 and M2 which are shown here in yellow and sky-blue colours. For pure systems, i.e. M1=M2, the number of configurations are reduced to only 9 as configuration 10 is identical to configuration 4.

2 Results and discussion

Spin states of all atoms, dimers and the GM of the free and supported clusters generated by MEGA, were optimized within VASP. All the pure and bimetallic species were found to exhibit the lowest possible spin state: singlet states for even-*N* clusters (which have an even number of electrons) and doublet states for odd-*N* clusters (which have an odd number of electrons). Figures S1 and S2 in the Supporting Information show the optimal spin state for each species as a function of their relative energies.

2.1 Structures

2.1.1 Free clusters

2.1.1.1 Pure clusters

The putative global minima for pure Au and Cu clusters $3 \leq N \leq 10$, are shown in Figure 3 and their energies and point groups are listed in Table S1 (see the Supporting Information).

The GM of the free Au clusters studied here are found to have 2D configurations, as previously reported [69–74]. Au_3 has a bent geometry, with a bond angle of 138.8°, in agreement with previous studies. 2D geometries are favoured for Au due to relativistic effects [75] which strengthens s–d hybridization by decreasing the 5d–6s energy separation.

Two generic structure types can be identified for Cu clusters: planar structures for up to 6 atoms which are identical to the corresponding Au clusters, except for Cu_3, which has an equilateral triangular structure, and 3D structures for $7 \leq N \leq 10$ which mostly favour deltahedral (triangular faced) compact configurations. The geometries obtained for Cu_N (N=4-7) agree with the findings of previous studies [76–80]. However, there are some differences. For clusters of size N=3, Li et al.[76], Jaque et al. [77] and Ramirez et al. [78] have all reported a C_{2v} symmetry isosceles triangle, while ours predicts a higher symmetry D_{3h} structure. For N=8, Ramirez et al. [78] and Li et al. [76] suggested a T_d symmetry tetracapped tetrahedron, while Jaque et al. [77] have reported a C_{2v} structure, which agrees with our findings. For Cu_9, though all previous and present calculations report a C_s symmetry structure as the GM, the structures are slightly different. The s-d hybridization, which is strong in Au clusters due to relativistic effects [75], is weaker for Cu, leading to 3D structures being favoured for copper when $N \geq 7$.

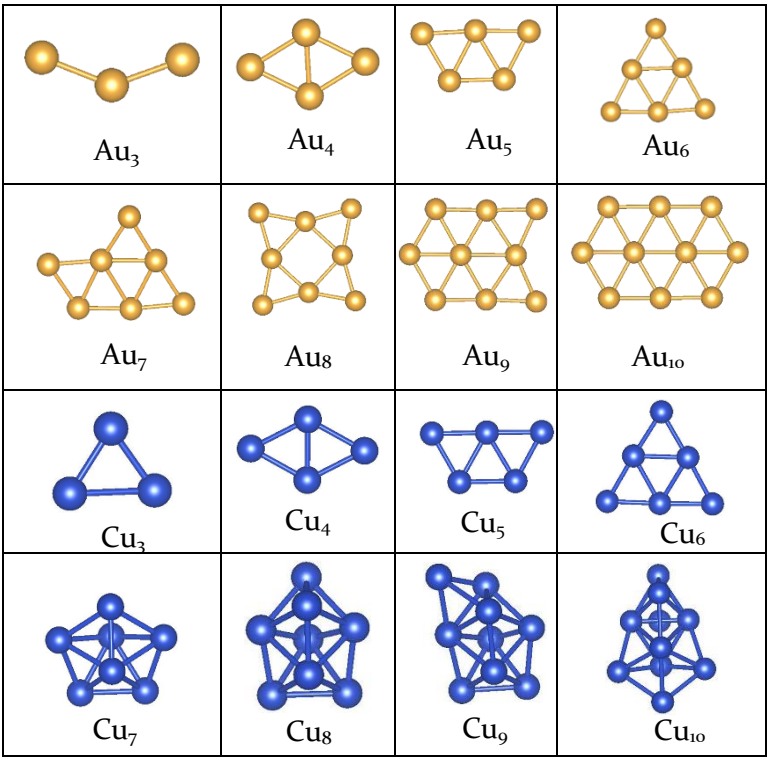

Fig. 3: Putative global minimum structures for Au_N and Cu_N clusters with N= 3-10. Au and Cu atoms are shown in gold and blue, respectively.

2.1.1.2 Bimetallic clusters

Fig. 4 shows the putative global minima for free bimetallic AuCu clusters. Their energies and point groups are listed in Table S2 (see the Supporting Information).

For Cu-doped Au clusters Au_mCu_1 (m=2-9), the planar structures of pure Au clusters are retained. Au_mCu_1 clusters have the same structures as the corresponding pure Au_{m+1} clusters, though Au_2Cu_1 has a closed triangular structure, rather than the bent structure of Au_3. All the GM of the Au-doped Cu clusters Au_1Cu_n (n= 2-9) are similar to the pure Cu clusters of the same size (Cu_{n+1}), except for Au_1Cu_7, in which the doped-Au atom changes the structure from a Δ-dodecahedron to a tetracapped tetrahedron. Such dopant-induced structural changes have previously been predicted for larger AuCu clusters [81-82].

All Au_mCu_n nanoalloys are found to have 2D structures for N=3-6 atoms. For N=7-9, a 2D-3D structural transition occurs for clusters with more than two Cu atoms. The global minima of $Au_{8-n}Cu_n$ clusters, n=1-5, are in good agreement with the results

previously described by Heard and Johnston [35]. The significant difference between those findings and these is that they predicted Au_6Cu_2 to have a 3D structure, while the present study predicts a 2D structure. Au_2Cu_6 and Au_1Cu_7 were both predicted to be 3D by Heard and Johnston [35], as in the present study, though the predicted geometries are different. For N=9 atoms, a compact structure of a pentagonal bipyramid fused with a bicapped tetrahedron is the lowest energy isomer for Au_2Cu_7, Au_4Cu_5, Au_5Cu_4, and Au_6Cu_3 clusters, while Au_3Cu_6 is a tetrahedral tricapped octahedron. The GM of Au_7Cu_2, as for the pure and singly-doped 9-atom clusters, adopts the planar "arrow shaped" structure shown in Figure 4. Its two Cu atoms are located at high coordination sites. For N=10, all of the clusters with more than a single Cu atom adopt 3D structures. A bi-capped Δ-dodecahedron structure is the GM for both Au_2Cu_8 and Au_3Cu_7. The GM of both Au_4Cu_6 and Au_5Cu_5 is a tetrahedral tetracapped octahedron, while for Au_6Cu_4, Au_7Cu_3 and Au_8Cu_2 they are derivatives of capped pentagonal bi-pyramids.

Considering the structures of the AuCu clusters shown in Figure 4, there is a strong tendency for Cu atoms to be located at interior, high-connectivity sites, as previously reported for larger clusters, which is due to the smaller size of Cu, the lower surface energy of Au and the better ability of the more electronegative Au atoms to stabilise the negative charge that tends to build up on exterior, low-coordinate sites [83–85]. These arguments also explain why Cu-deficient clusters tend to maximise Cu-Cu bonding at the core of the cluster, while Au-deficient clusters tend to have isolated Au atoms occupying peripheral sites. This also suggests a chemical order of Cu-core Au-shell for larger clusters [81].

2.1.2 Supported clusters

2.1.2.1 Supported atoms and dimers

The adsorption energies of Au and Cu adatoms on MgO(100) are listed in Table 1 and shown graphically in Figures S3-S5 (see Supporting Information). Table S3 in the Supporting Information lists the energies of free and supported atoms and dimers. After DFT minimisation, all Au and Cu adatoms remained on their initial sites, except for those initially bridging a Mg-O bond, which (for both Au and Cu) relax onto an oxygen atom (O-site). The O-site is the most favourable adsorption site for both Au and Cu. There is a slightly more negative adsorption energy (corresponding to stronger M-O binding) for Cu (-0.92 eV) than for Au (-0.90 eV) on the O-site. On the O-site, the calculated zero-point energy (at the harmonic level) is higher by 0.01 eV for a Cu adatom than for an Au adatom, resulting in the Cu-O adsorption energy being very close to Au-O (approximately 0.01 eV). The closeness in M-MgO binding (adsorption) energies on the O-site, for M = Cu and Au, has also been calculated theoretically by Neyman et al. [86a], and the difference (and order) was found to be dependent on the xc functional. We have also checked the effects of the relaxation of the substrate: (i) allowing the upper most MgO layers to relax (always keeping the lowest MgO layer fixed to impart some bulk like rigidity); (ii) allowing all the MgO layers atoms to relax. These calculations also

suggest a very small difference between the adsorption energies of Cu and Au adatoms in both cases (0.07 eV for upper layer relaxation and 0.06 for both layers relaxed), with the Cu atom being slightly more strongly bound in each case. Taking into account the effect of zero-point energy and substrate relaxation, the Cu and Au adatom adsorption energies are almost identical. The Mg and H sites are local minima for adatom adsorption, with stronger adsorption (more negative E_{ads}) observed for the larger, more polarisable Au atom.

The adsorption energies of Au_2, Cu_2 and AuCu dimers, starting from vertical (V) and parallel (P) orientations, are shown in Tables 1 and 2, respectively, and are shown graphically in Figures S4 and S5 in the Supporting Information. In contrast to the adatoms, Au_2 dimers are adsorbed more strongly (i.e. have more negative E_{ads} values) than Cu_2 dimers for all sites, in both the V and P orientations. The O-site is preferred for both Au_2 and Cu_2. The bridge site changes to the O-site, as for the adatoms. Both dimers, when initially placed on P site 4 (see Figure 2), relax after DFT minimization to the O-site V configuration, which has a lower energy than all the P configurations. The most stable P configuration generally maximizes metal-oxygen (M-O) bonds and elongates the metal-metal (M-M) bond, thus weakening the M-M interaction, as the M-O bonding competes with M-M bonding. In contrast, due to the metal-on-top effect [86b], the V configurations exhibit both stronger M-O and M-M bonding, as listed in Table S4 in the Supporting Information. The reason for the unexpected greater adsorption strength of Au_2 than Cu_2 in the V configurations (in contrast to the trend for the Cu and Au adatoms) is because the metal-on-top effect is greater for Au than Cu, due to the greater polarizability of Au [86b].

On the MgO(100) surface, as for the pure dimers, the AuCu dimer also favours V configurations (with the O-site again being the preferred binding site), but the Cu-adsorbed configurations (Au on top of Cu) are more favourable than Au-adsorbed configuration (Cu on top of Au). This can be explained by the Cu-O interaction being stronger than Au-O: the adsorption energy calculated for a Cu adatom on the O-site is larger in magnitude (by approximately 0.02 eV) than the Au adatom (see Table 1). For the Cu-adsorbed AuCu dimer, the Cu-O bond is further strengthened because the greater electronegativity of Au (compared with Cu) atom results in electron transfer from Cu to Au, leaving a positively charged Cu atom, which binds more strongly to the oxide anion. As shown in Table 1, the order of dimer adsorption energies (for the O-site V configuration) is as follows: **Au**Cu < Cu**Cu** < Au**Au** < Au**Cu** (where the bold atom is bound to the O-site). The weaker Au-adsorbed configuration of AuCu (relative to Au_2) can be explained by the Cu to Au electron transfer weakening the Au-O binding and the weaker metal-on-top effect with Cu above Au. Many P configurations of the AuCu dimer (interestingly, not including site 4) relax after local DFT minimization to the (O-site) V configuration, forming a Cu-O bond.

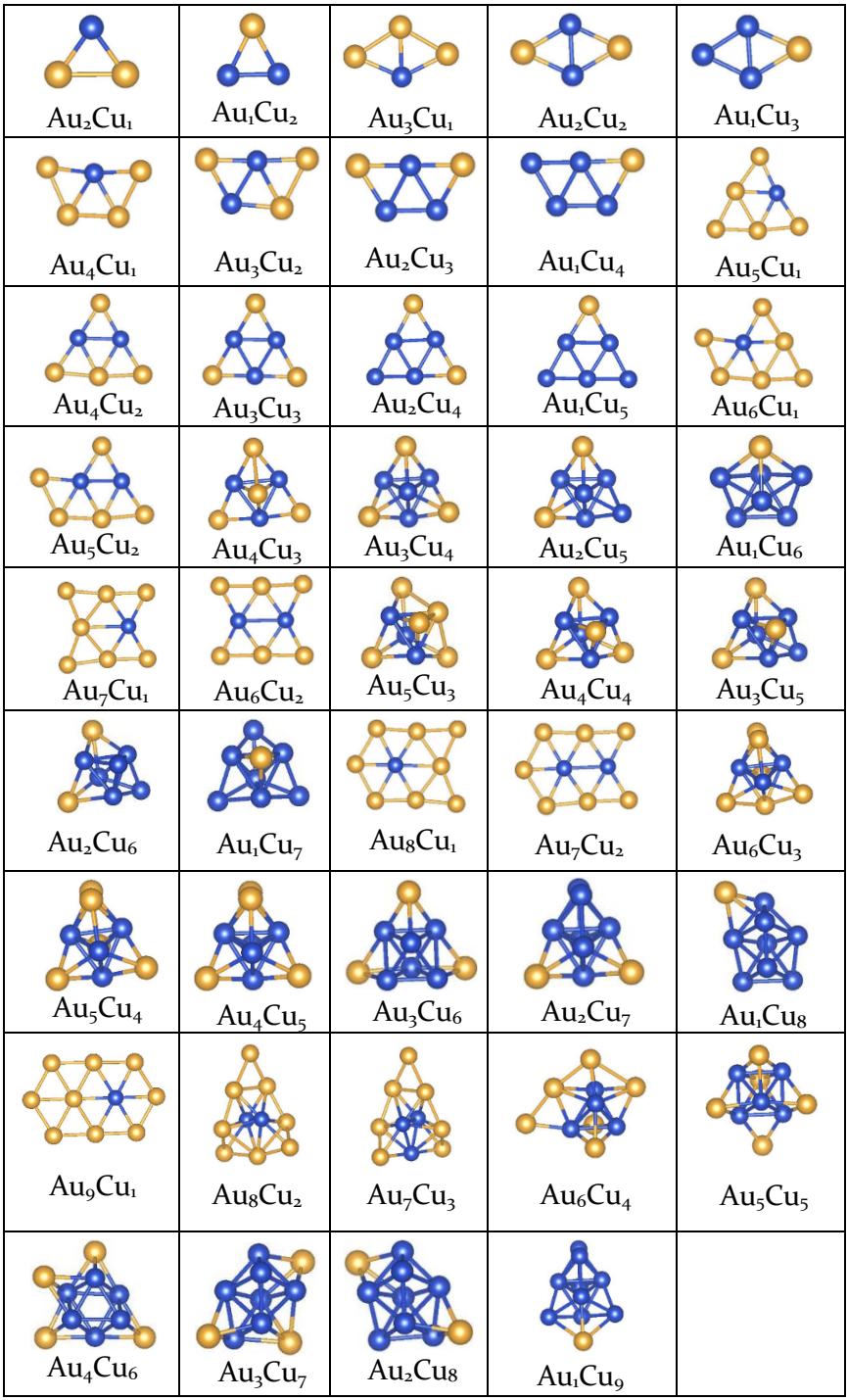

Fig. 4: Putative global minimum structures for all compositions of free AuCu nanoalloys with sizes N = 3-10.

2.1.2.2 Supported pure metal clusters

As has previously been discussed [70,87,88], Au_4 adopts an elongated planar rhombus structure on the surface because the Au-O bonding increases the distance between the two Au atoms that are in contact with the surface from 2.6 Å to 3.7 Å and increases the bond angle from (60.9°) to (90.5°). The structure of surface-supported Au_5 also has an elongated Au−Au bond spanning two O atoms. However, the reverse is observed for Au_3, as its interaction with the surface reduces the bond angle from (138.8°) in the gas-phase to (80.9°). It is interesting that these three clusters are the only ones where two metal atoms bond to two oxygen atoms across an O-Mg-O edge of the MgO(100) surface, due to the distorted cluster structures having relatively long Au-Au distances. In the larger Au clusters (as well as the Cu and AuCu clusters), any distortions are smaller (presumably because larger bond distortions would destabilise the cluster too much), so the M-M bonds bridge across a diagonal of a Mg_2O_2 square on the Mg(100) surface.

As is commonly seen in such clusters, due to "metal-on-top effect" [86b] the MgO-supported GM structures are all found to lie perpendicular to the plane of the surface. Our MEGA search for supported Au clusters is in excellent agreement with our previous search using the BPGA code [70], except for the supported Au_8 cluster, for which the GM found here is 0.14 eV lower in energy than the previously proposed structure (a tetracapped square, as in the gas-phase GM). It should be noted that up to N=7, the structures of the supported clusters are essentially the same as in the gas-phase (with some distortions, as mentioned above), whereas the structures of the larger clusters (N=8-10), although still planar, have different structures on the surface compared to the gas-phase.

Although Cu_3 and Cu_4 clusters retain their gas-phase structures on the surface, the other oxide-supported Cu clusters deviate from planarity for N≥5 and distort to give more complex fused structures.

Table 1: Adsorption energies for all adatoms and dimers on MgO(100), with the dimers starting from V configurations. The lowest E_{ads} value is shown in bold font for each molecule/orientation. For the AuCu dimer, the atom on the surface is indicated in bold font. Position 1 is not included, as all adatoms or dimers initially placed on position 1 relaxed to position 4.

Position	E_{ads} (Au)/eV	E_{ads} (Cu)/eV	E_{ads} (AuAu)/eV	E_{ads} (CuCu)/eV	E_{ads} (**Au**Cu)/eV	E_{ads} (Au**Cu**)/eV
2	-0.68	-0.48	-0.78	-0.57	-0.55	-0.76
3	-0.48	-0.42	-0.31	-0.17	-0.20	-0.23
4	**-0.90**	**-0.92**	**-1.42**	**-1.26**	**-1.03**	**-1.55**

Table 2: Adsorption energies for all dimers on MgO(100) starting from P configurations. The numbers in italics indicate those configurations that transform to the O-site V configuration after energy minimisation. The most negative values of E_{ads} are shown in bold font.

Position	E_{ads} (AuAu)/eV	E_{ads} (CuCu)/eV	E_{ads} (AuCu)/eV
1	-0.51	-0.21	*-1.54*
2	-0.70	-0.70	-0.79
3	-0.70	-0.70	***-1.57***
4	***-1.39***	***-1.22***	-0.55
5	-0.47	-0.46	-0.65
6	-0.39	-0.21	-0.29
7	-0.56	-0.92	***-1.57***
8	-0.31	-0.19	*-1.54*
9	-0.49	-0.92	*-1.55*
10			*-1.53*

2.1.2.3 Supported bimetallic clusters

The structures of supported Au_mCu_1 clusters are found to be similar to their gas-phase equivalents for sizes N=3 and N=5-7 atoms, while they are different from their gas-phase analogues for N=4 and N=8-10 atoms. For N=4, the structure is similar to the pure supported Au cluster, having an elongated Au-Cu bond bridging two O atoms on the surface. Even though the supported Au_6Cu_1 cluster has the same overall geometric structure as the corresponding free cluster (a 6-atom triangle with an extra bridging atom), there is a clear change in the homotop as the unique Cu atom moves from the most highly coordinated 5-connected site to a 4-connected site, to allow it to bind to an O atom of the surface. We have assessed two alternative structures (both having the same trapezium geometry and having Cu at the cluster-surface interface) to confirm that our supported Au_4Cu_1 cluster (which has the same structure and homotop as in the gas-phase) is the true GM (Figure 8b). Although Au_7Cu_1 retains its 2D structure on the surface, it is totally different from the corresponding free cluster (a tetra-bridged rhombus) but the same as the supported Au_8 cluster. The Cu atom is located at a high (4) connectivity site and binds to a surface O atom. The GM of supported Au_7Cu_1 is lower in energy (by between 0.15 and 0.53 eV) than its homotops, as shown in Figure S6 (Supporting Information). The supported Au_7Cu_1 structure is extended by one more Au atom to form the supported Au_8Cu_1 cluster, which is again different from the gas-phase, structure, though both are 2D. The lowest competitive isomer for the GM of Au_8Cu_1 (with a relative energy of 0.28 eV) is also 2D, as shown in Figure 8e. Supported Au_9Cu_1 is a composite structure made up by fusing the free Au_5Cu_1 and Au_8 structures, generating a planar Cu-centred isomer on the surface. As it is possible that MEGA-DFT missed a lower energy homotop, we constructed some alternative arrangements for supported Au_9Cu_1 and locally minimised them at the DFT level, as shown in Figure S6 (Supporting Information). As a result of this study, we are confident that our reported structure is the true GM.

For singly Au-doped Cu clusters, the structures on the surface are found to be different from their gas-phase counterparts, except for sizes N=3-6 atoms, but Au_1Cu_2 is found to have an elongated Cu-Cu bond on the surface. Supported Au_1Cu_{N-1} clusters agree with their free counterparts in showing a structural transition from 2D to 3D at N=7. The nearest competitive isomer to the GM of Au_1Cu_3 has the same rhombus structure, but is a homotop, with the Au atom at a 3-connected, rather than the preferred 2-connected site (as in the gas phase), with a relative energy of 0.42 eV (Figure 8c). The proposed GM of Au_1Cu_4 has been compared with an alternative homotop, with the same underlying trapezium geometry (Figure 8d) but with the Au atom in a 3- rather than 2-connected site and the trapezium oriented the other way up on the surface. Interestingly, the second homotop, which in the gas-phase is significantly destabilized with respect to the GM, is only 0.02 eV higher in energy on the surface, as it has a greater number of Cu-O bonds. Free Au_1Cu_6 has a pentagonal bipyramid structure, as for pure Cu_7 whereas the GM is a tri-capped tetrahedron on the MgO surface. The tri-capped trigonal bipyramidal structure of the free Au_1Cu_7 cluster distorts on the surface to form a fused square-based pyramid with a trigonal bipyramid. The free Au_1Cu_8 has the capped Δ-dodecahedron structure of Cu_9 but they have different compact structures on the surface. For N=10, the putative GM of Au_1Cu_9 and Cu_{10} cluster have identical structures in the gas-phase and when supported, though the gas-phase and supported structures are slightly different.

For AuCu clusters of other compositions, the most stable structures for N=4 are all found to form rhombic structures which remain essentially the same on the surface (albeit with some degree of M-M bond lengthening, as mentioned above). The trapezoidal structure found for all mixed-cluster compositions with N=5 is still the GM for their supported species. Two competitive isomers were evaluated against the putative GM of Au_2Cu_3 and Au_3Cu_2 showing that our GM are lower in energy by 0.31 eV and 0.05 eV, respectively, as seen in Figures 8f and 8g. Again, it is interesting to note that the inverted orientation of the trapezium (having only 2 atoms in contact with the substrate) is favoured in both cases, even (as shown in Figure 8f) when the 3 atoms at the interface are all Cu atoms (which form stronger bonds to O). For N=6, the planar triangle is the GM for all the gas phase clusters and all but one of the MgO(100)-supported clusters: the supported Au_2Cu_4 cluster is a capped trigonal bipyramid. The latter was evaluated against an alternative planar triangle isomer, as shown in Figure 8h, with our putative GM predicted to be more stable by 0.08 eV. For both supported Au_4Cu_2 and Au_3Cu_3, there are two adjacent Cu atoms on the bottom edge of the triangle, binding to surface O atoms. Figure 8i shows a comparison of the putative GM for supported Au_4Cu_2 with an alternative triangular structure with only one Cu at the interface (having a relative energy of 0.17 eV) and with a 2-layer parallelogram structure (1.21 eV above the GM). Figure 9 shows a comparison of the energies of three alternative homotops of triangular Au_3Cu_3 (all having at least 2 Cu-Cu bonds), as well as the 2-layer parallelogram consisting of a chain of 3 Cu atoms and one of 3 Au atoms. In the gas-phase, the most symmetrical triangular homotop, which has a central Cu_3 triangular core, is favoured by at least 0.53 eV compared to the other homotops, while the parallelogram structure is destabilised by 2.11 eV relative to the GM. When binding to the surface via the Cu_3 edge, this isomer (which was found to be the GM for the MgO-supported Au_3Pd_3 cluster [70]), has the

highest (magnitude) adsorption energy (E_{ads}) of -3.24 eV (compared to only -1.68 eV for the gas-phase GM). The triangular homotop with a Cu_3 edge also binds strongly to the surface via this edge (E_{ads} = -2.77 eV) and corresponds to the GM for the MgO-supported Au_3Ir_3 cluster [88]. However, the GM for the supported Au_3Cu_3 cluster (stabilised by 0.08 eV relative to the supported gas-phase GM) has 2 Cu atoms in contact with the surface and an adsorption energy of -2.35 eV.

Doping more than two Cu atoms changes the structures of both gas-phase and supported Au_7 from an edge-bridged planar triangle (which is also found when doped with 1 or 2 Cu atoms) to 3D structures. In the gas-phase, the tricapped tetrahedron is found for Au_4Cu_3 to Au_2Cu_5 (with Cu atoms preferentially occupying the inner tetrahedron sites). This structure is maintained for supported Au_4Cu_3 and Au_3Cu_4, but supported Au_2Cu_5 has a Cu_5 square-based pyramid capped on two triangular faces by Au atoms, binding to the MgO surface via the square of 4 Cu atoms, which has a good epitaxial match with the MgO(100) surface. Interestingly, as shown in Figure 8j, Au_4Cu_3 binds to MgO via the formation of only two Cu-O bonds, with a Au atom slightly further from the surface, which is preferred by 0.44 eV over the orientation with the third Cu atom close (but not bonded) to the surface.

In the gas phase, Au_6Cu_2 (like Au_7Cu_1) adopts a rhombic distortion of the 2D Au_8, but it forms a 3D structure on the MgO surface. 8-atom AuCu clusters with more than two Cu atoms all have 3D tetracapped tetrahedron structures and the supported clusters are distorted to form 3D structures composed of fused square based pyramid derivatives. Assessing the effect of homotop swapping for supported Au_6Cu_2 and Au_4Cu_4 clusters (Figures 8k and 8l) give us confidence that the lowest energy structures reported here are the true GM for both compositions.

All supported AuCu clusters with N=9, except Au_7Cu_2, are predicted to be square-based pyramids capped or bridged by predominantly Au atoms. The GM of supported Au_7Cu_2 is a folded pseudo-planar structure. All supported AuCu clusters with N=10 are capped square-based pyramid derivatives, except for Au_7Cu_3 and Au_8Cu_2 which have quite flat bi-layer structures parallel to the surface.

The differences between the energies of the Mg(100)-supported GM and the energies of the supported clusters with the slab removed represent the E_{ads} for such systems. Tables S5 and S6 (see the Supporting Information) list the E_{ads} of the supported clusters and Figure 10 shows a graphical representation. The plots show that Cu clusters with N=5-10 have more negative E_{ads} (stronger cluster-surface binding) compared with the corresponding Au clusters, due to the stronger Cu-O interactions. 3- and 4-atom pure Cu clusters, however, exhibit weaker binding to the surface (less negative E_{ads}) than for Au. This may be attributed to the ability of Au_3 and Au_4 to deform significantly on the surface (either lengthening or shortening Au-Au contacts) to enable enhanced Au-O interactions.

Comparing the E_{ads} values for the mixed AuCu clusters as a function of size and composition is more complicated, but, in general, it is found that the 3D structures exhibit stronger adsorption (more negative E_{ads} values) compared with 2D clusters of the same size. This is due to the interplay between the number of interfacial atoms (especially Cu, which forms stronger M-O bonds than Au) and the relative stabilities of the 2D and 3D

structures in the gas-phase. The elongation of M-M bonds on the surface, which is observed for some smaller Au and Au-rich clusters, also gives more flexibility for clusters to form stronger M-O bonds with the surface. For example, for N=3 and 4, the distorted Au_1Cu_2 and Au_3Cu_1 clusters have the most negative E_{ads} values of all the mixed clusters at these sizes. Consistent with their structures, E_{ads} of Au_4 is found to be equal to that of Au_3Cu_1. The unique 3D structure of supported Au_2Cu_4 among the 6-atom AuCu clusters is consistent with it having the most negative E_{ads}, due to forming 3 Cu-O bonds. For N=7-9, supported Au_2Cu_5, Au_3Cu_5, and Au_5Cu_4 clusters have the most negative E_{ads} values. All these clusters have supported structures based on fused square-based pyramids, mostly formed from Cu atoms, with mainly capping Au atoms. Due to the greater electronegativity of Au, there is Cu to Au electron transfer, which strengthens the Cu-O interactions. An even-odd alternation in adsorption energies is observed for supported 10-atom AuCu clusters, with more negative values (indicating stronger adsorption) for clusters containing even numbers of Au atoms (and, hence, even numbers of Cu atoms). Au_8Cu_2 has the most negative E_{ads}, perhaps because the two Cu atoms are more exposed to the MgO surface as they lie below the pseudo-planar Au_8 fragment. Au_9Cu_1, which has no Cu-O interactions, has the least negative E_{ads}. The slightly more negative value of E_{ads} calculated for Au_{10} may be because the Au-Au bonds are more easily deformed in the homonuclear cluster, enabling stronger interaction with the surface O atoms. It is not clear why this even-odd alternation is seen, nor why it is not observed over the entire composition range for the other cluster sizes.

2.2 Energetic analysis

As explained earlier, the preferred locations for Au atoms in AuCu nanoalloys are at low coordination surface sites (i.e. at edges, vertices and capping sites), while Cu atoms in such systems tend to be located at high coordination core sites. Structural preferences and cluster stability can be explained by calculating the excess (or mixing) energy (Δ), the binding energy (E_b) and the second difference in energy (Δ_2E), which are defined in Eqns. (7)–(9). Tables S5 and S6 (Supporting Information) list the values of these energies for all AuCu systems studied here.

The relative stabilities of pure and singly doped clusters of different nuclearities can be determined from the second difference in energy (Δ_2E), which indicates the stability of an N-atom cluster with respect to neighbouring sizes. Figure S7 in the Supporting Information shows plots of the second difference in energy Δ_2E for pure Au and Cu clusters, mono-substituted clusters and their supported clusters as a function of cluster size. Relatively stable clusters are represented by positive peaks in Δ_2E. For pure metal clusters, Au_6 (planar) and Cu_8 (3D) clusters have the highest relative stabilities compared to their neighbours. Thus N=6 and N=8 indicate magic sizes for 2D Au clusters [70] and 3D Cu clusters, respectively. The fact that the binding energy of Au_6 is higher than Au_7 (as discussed below) also supports this hypothesis. The plots also show that when the total number of atoms in a cluster is even (for pure or mono-substituted clusters), Δ_2E is positive and relatively high, whereas it is negative for clusters with odd numbers of atoms. This even-odd alternation is consistent with the electronic shell model

[89-92], which predicts enhanced stability for even-electron clusters, corresponding to an even number of atoms, since each Au or Cu atom contributes one (6s or 4s) electron towards the delocalised cluster bonding. Doping a single Cu atom into Au clusters does not change the relative stability of the most stable size (N=6), while it reduces the relative stability of N=8 and enhances that of N=4. The highest peak for pure Cu clusters occurs at N=8, which remains the highest peak after doping one Au atom. Supporting the pure Au and Cu clusters on MgO(100) does not change the $\Delta_2 E$ trend found for the gas-phase clusters. For mono-substituted supported clusters, the same odd-even alternation in stability is seen as for the unsupported clusters.

As mentioned above, the electronegativity difference between Cu and Au leads to electron charge transfer from Cu to Au, which favours Au-Cu mixing. The effect of Au-Cu mixing on the stability of the mixed clusters can be investigated by calculating the mixing/excess energy (Δ). Plots of the excess energy for Au-Cu clusters (N=2-10) are shown in Figure S8 in the Supporting Information. Negative values of Δ indicate a high mixing tendency, while positive values indicate unfavourable mixing. For all clusters with N=2-10, mixing is favoured. The maximum mixing tendency (most negative Δ values) is achieved for Au/Cu ratios of 1 (or close to 1, for odd-atom clusters). The excess energy values for clusters with the same size shows that composition variation plays a more important role in determining cluster stabilities than geometric effects. Generally, larger clusters have more negative Δ values, for gas-phase clusters this corresponds to the Cu atoms preferentially entering the highly-coordinated core-like sites. For even larger clusters, this leads to core-shell segregation, consistent with the structures predicted by Darby et al. [81a] using an empirical potential and Goh et al. [81b] using an atomistic many-body potential.

Relative cluster stabilities can also be obtained by calculating the binding energy per atom (E_b). Figure S9 in the Supporting Information shows the binding energies for AuCu clusters plotted against the Au proportion. Higher binding energy indicates higher stability. As expected, due to the increase in the average number of metal-metal bonds, the binding energy generally increases with increasing cluster size, as previously reported for different metallic systems [70, 71, 93, 94]. Pure Au clusters are relatively less stable (having lower E_b values) than pure Cu clusters of the same size. For the mixed clusters, the plot also shows that the most stable compositions are found as the Au/Cu ratio approaches 1, which is consistent with the excess energy plots.

The chemical stabilities of the clusters can be investigated by analysing their HOMO-LUMO energy gaps (Δ_{HL}), with large Δ_{HL} indicating high stability of the system with respect to oxidation (corresponding to a low-lying HOMO) and reduction (corresponding to a high-lying LUMO). Figure 11 shows plots of Δ_{HL} as a function of the total number of atoms (N) for pure and mono-substituted clusters and for their oxide-supported counterparts. All of the Δ_{HL} plots show marked odd-even alternations, with larger Δ_{HL} values for even-atom (and, hence, even-electron) clusters and smaller values for odd-atom (odd-electron) clusters. This behaviour has previously been explained in terms of the electronic shell model [93-99].

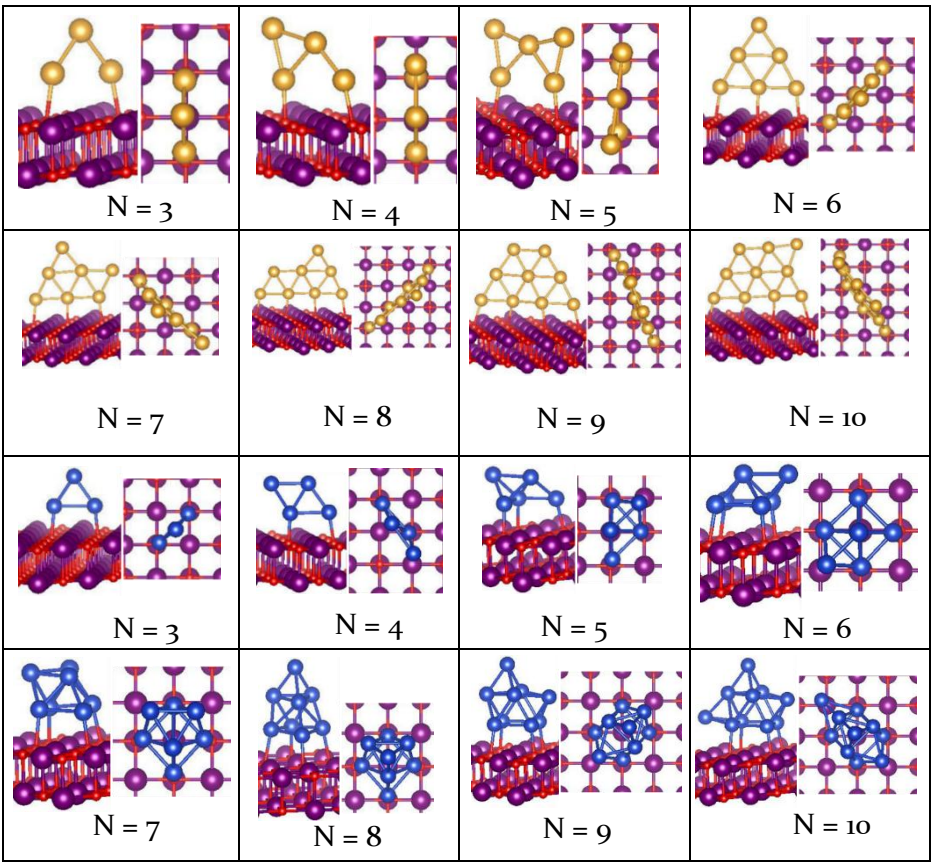

Fig. 5: Putative global minimum structures for MgO(100)-supported Au_N and Cu_N clusters with N= 3-10.

For the free pure and mono-substituted clusters, N=6 and N=8 tend to have the highest Δ_{HL} values, which is consistent with the Δ_2E plots, since high HOMO-LUMO gaps typically correlate with low total electronic energy (stabilisation of filled orbitals). The stability of 6- and 8-electron clusters has previously been discussed for neutral Au_6 and Au_8 and the cationic Au_7^+ and Au_9^+ clusters [14]. Doping a single Cu atom into the Au clusters (Figure 11a) leads to a decrease in Δ_{HL}, with the exception of $Au_4 \rightarrow Au_3Cu_1$, where there is a significant increase in Δ_{HL}. Doping a single Au atom into the Cu clusters (Figure 11b) leads to an increase in Δ_{HL} for N = 2-4, 8 and 10, while there is almost no difference for N = 5 and 6 and a decrease in Δ_{HL} for N = 7 and 9.

The Δ_{HL} plots in Figure 11 (c-f) show that supporting the pure and mono-substituted clusters on the MgO surface increases the HOMO-LUMO gaps of the smaller clusters with N<5 atoms, while Δ_{HL} is generally decreased for the larger clusters. For N = 5, there is little or no difference in Δ_{HL} between the gas-phase and supported clusters. The increase in Δ_{HL} for the smaller clusters may be due to MgO to cluster electron transfer (see

below), leading to destabilisation of the empty cluster orbitals (including the LUMO), while the decrease in Δ_{HL} for the larger clusters probably reflects surface-induced changes in homotopic or geometric structures and, hence, changes in the cluster electronic structure. As shown in Figure 9, the cluster isomers which bind most strongly to the MgO surface are not always the most stable gas-phase structures, so it is not surprising that the HOMO-LUMO gap for the cluster-surface GM may be smaller than for the free gas-phase cluster GM.

As mentioned above, clusters with high HOMO-LUMO gaps are expected to show reduced reactivity. Hardness (η, Eqn. 4) [98-100] is an important descriptor for the stability and reactivity of a given system [101] and can be interpreted as the system's resistance to changing its electronic distribution or its electronegativity [102], and is also related to valence-conduction band transitions in optical spectroscopy [103]. The linear regression analysis from a plot of Δ_{HL} values for our free AuCu clusters against their computed softness ($S = 1/(2\eta)$, Eqn. 5), shown in Figures S10 and S11 (Supporting Information), confirms that the optical gaps for these clusters are directly proportional to their softness values.

It is well known that electrons should flow from lower electronegativity (χ) atoms to those of higher electronegativity (i.e. to lower the chemical potential). Our χ values (Eqn. 3) for most of the compositions reported in Tables S7-S10 in the Supporting Information, show a significant decrease in χ when the cluster is adsorbed on the MgO surface, which is consistent with electron transfer from the MgO surface to the cluster. The comparison of χ values for both free and supported clusters shows that Au and Au-rich clusters (with higher χ) hold their electrons more than Cu and Cu-rich clusters. The decrease of the electrophilicity (ω, Eqn. 6) values of clusters when supported on the MgO surface is also consistent with the surface acting as an electron donor.

3 Conclusions

We have used the DFT-based Mexican Enhanced Genetic Algorithm (MEGA-DFT) to locate the global minima of gas-phase and MgO(100)-supported Au, Cu, and AuCu clusters with 3-10 atoms. We have also performed local energy minimisations of supported metal adatoms and dimers. The ability of the MEGA-DFT approach in searching for putative global minima has been successfully assessed using a systematic homotop search method for some selected clusters and reminimisation calculations for alternative potentially competitive isomers.

The GM reported here for free AuCu nanoalloys show that 2D structures are found to be the predominant motifs for 3-6-atom AuCu clusters, whereas a 2D-3D crossover is observed when doping more than two Cu atoms into 7-9 Au clusters and doping more than one Cu atom into Au_{10}. There is a high tendency for Cu atoms to be located at interior high-coordinate sites. This can be attributed to the larger size of Au atoms and the lower surface energy of Au, as well as the ability of the more electronegative Au atoms to stabilise the negative charge that tends to build up on low-connectivity peripheral sites. As a result, Cu-deficient clusters tend to maximise Cu-Cu bonding at the centre of the cluster, while Au-deficient clusters tend to have isolated Au atoms occupying exterior sites. Calculated excess and binding energies confirm this conclusion, showing that the highest mixing tendency is

found close to a Au/Cu ratio of 1. Accordingly, core-shell segregation is the predominant chemical ordering for these clusters and is also predicted for larger nanoparticles.

On the MgO(100) surface, the O-site is the most favourable adsorption site for both adatoms and dimers. Au and Cu adatoms remain on their initial positions, except for those initially bridging a Mg-O bond, which relax to an atop oxygen site (O-site). The higher affinity of a Cu atom for the O-site is reflected in the more negative adsorption energy ($\Delta E_{ads} \approx -0.02$ eV) for Cu compared to Au. All adsorbed dimers favour vertical (V) configurations due to the metal-on-top effect. In line with the results for adatoms, the supported AuCu (V) dimers show stronger adsorption for Cu-adsorbed configurations (Au on top of Cu). The Cu-O bond is further strengthened because the lower electronegativity of Cu (compared with Au) results in electron transfer from Cu to Au, and the positively charged Cu atom binds more strongly to the oxide anion. However, the situation is different for pure metal dimers: due to the greater metal-on-top effect (greater polarizability) of Au compared with Cu, Au_2 has a more negative adsorption energy than Cu_2. The resulting order of adsorption strength for the dimers is: **Au**Cu < Cu**Cu** < Au**Au** < Au**Cu** (where the bold atom is bound to the O-site).

The core-shell segregation pattern of free AuCu nanoalloys is broken when supported on the MgO(100) surface, due to a homotop switch whereby more Cu atoms tend to aggregate at the oxide interface. For small supported Au and Au-rich clusters, the bond-elongation effect enhances the metal interactions with O atoms of the surface rather than strengthening the M-M bonding, as is observed in the smaller Cu clusters. This can lead to enhancement of the stability of Au-adsorbed configurations in these clusters.

The higher relative stabilities for free and supported even-number clusters, corresponding to peaks in $\Delta_2 E$ and Δ_{HL}, compared to their odd-numbered neighbours, reflects the enhanced stability of closed-shell even-electron clusters, since each Au or Cu atom contributes its single valence s electron to cluster bonding. The computed electronegativity and electrophilicity indices for free and supported Au and Au-rich clusters reveal that such clusters hold their electrons more tightly than other clusters of the same size. The analysis also shows that there is electron transfer from the MgO surface to the adsorbed metal cluster. For the bimetallic clusters, adsorption is found to reduce the extent of Cu to Au electron transfer.

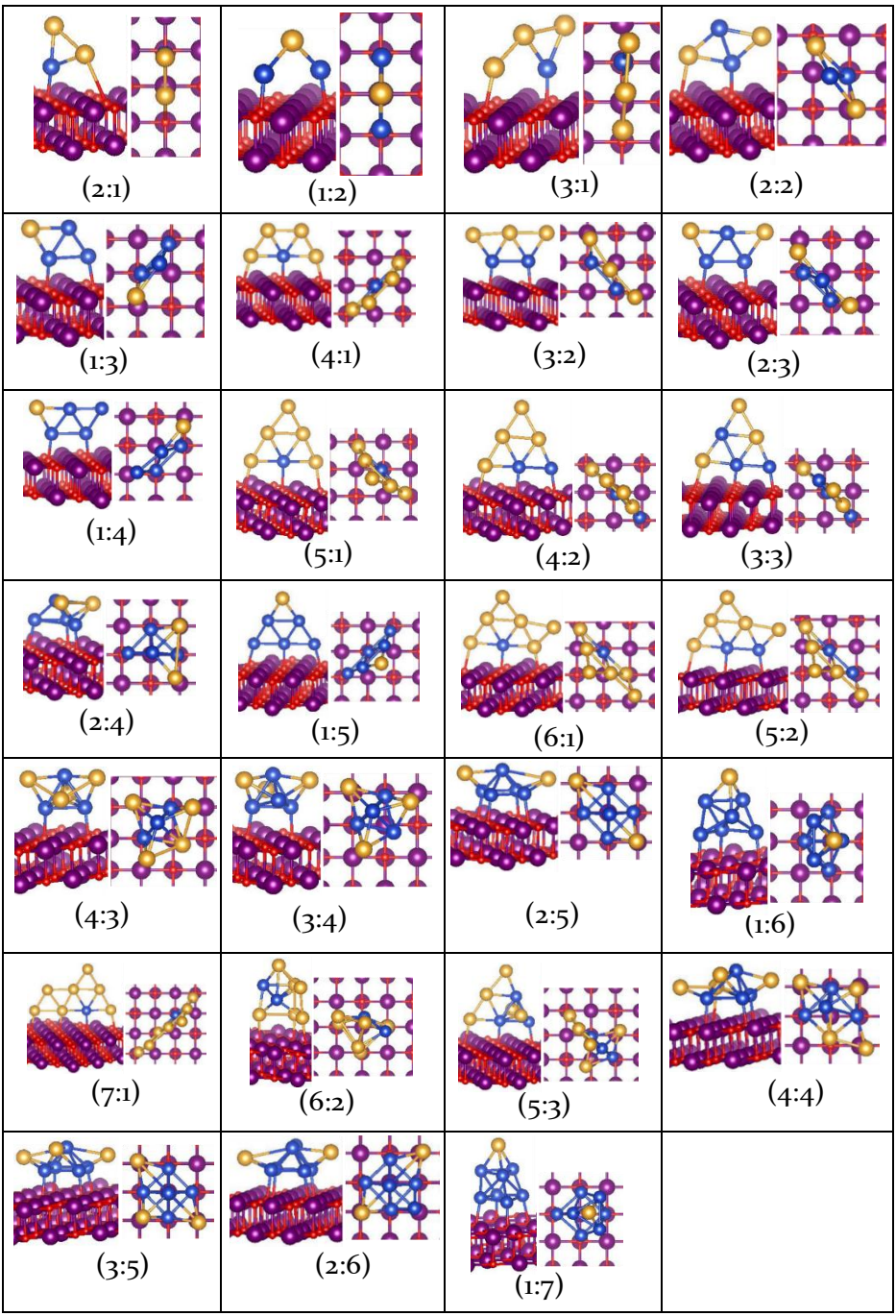

Fig. 6: Putative global minimum structures for all compositions of MgO(100)-supported AuCu clusters with N= 3-8.

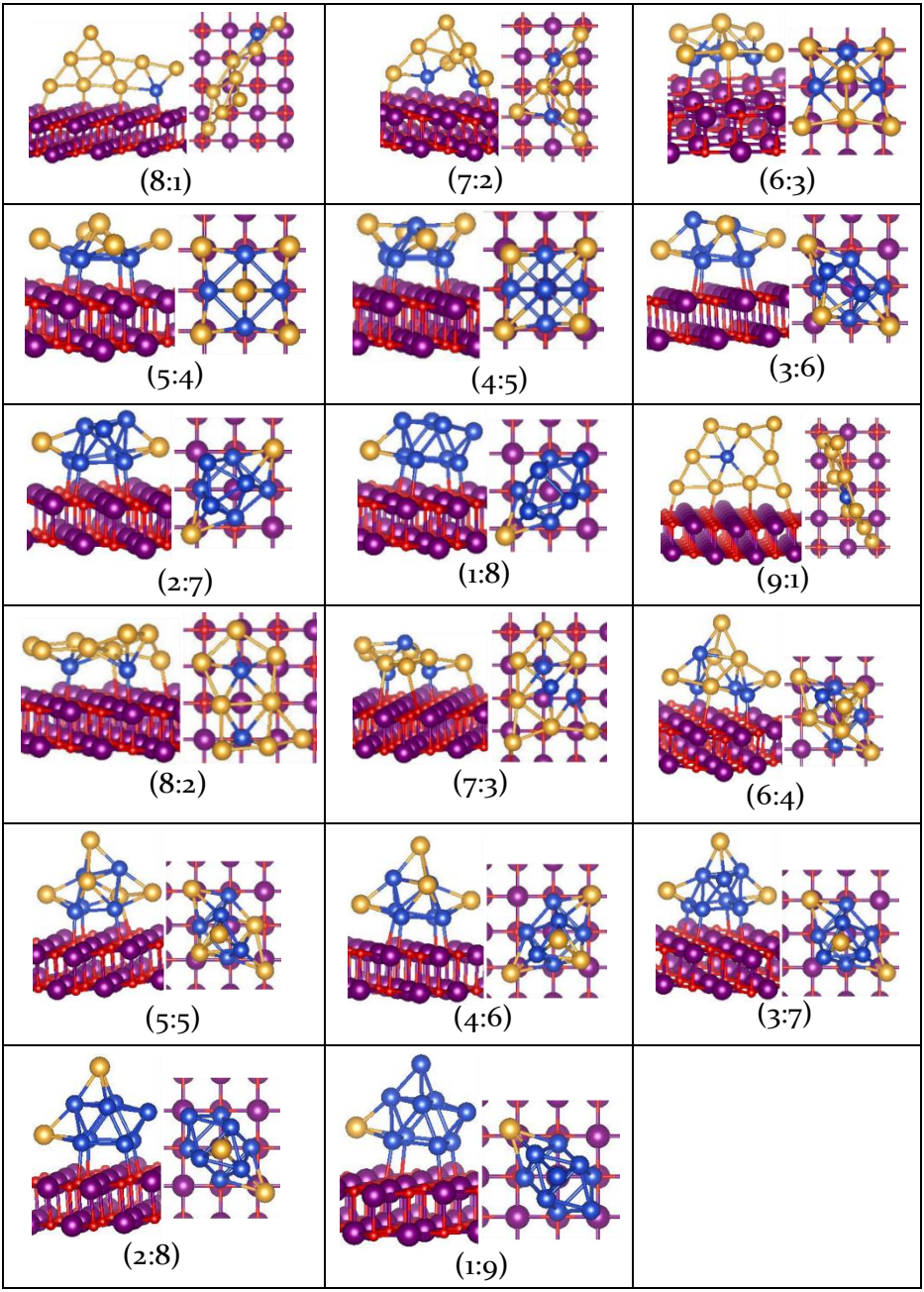

Fig. 7: Putative global minimum structures for all compositions of MgO(100)-supported AuCu clusters with N= 9 and 10.

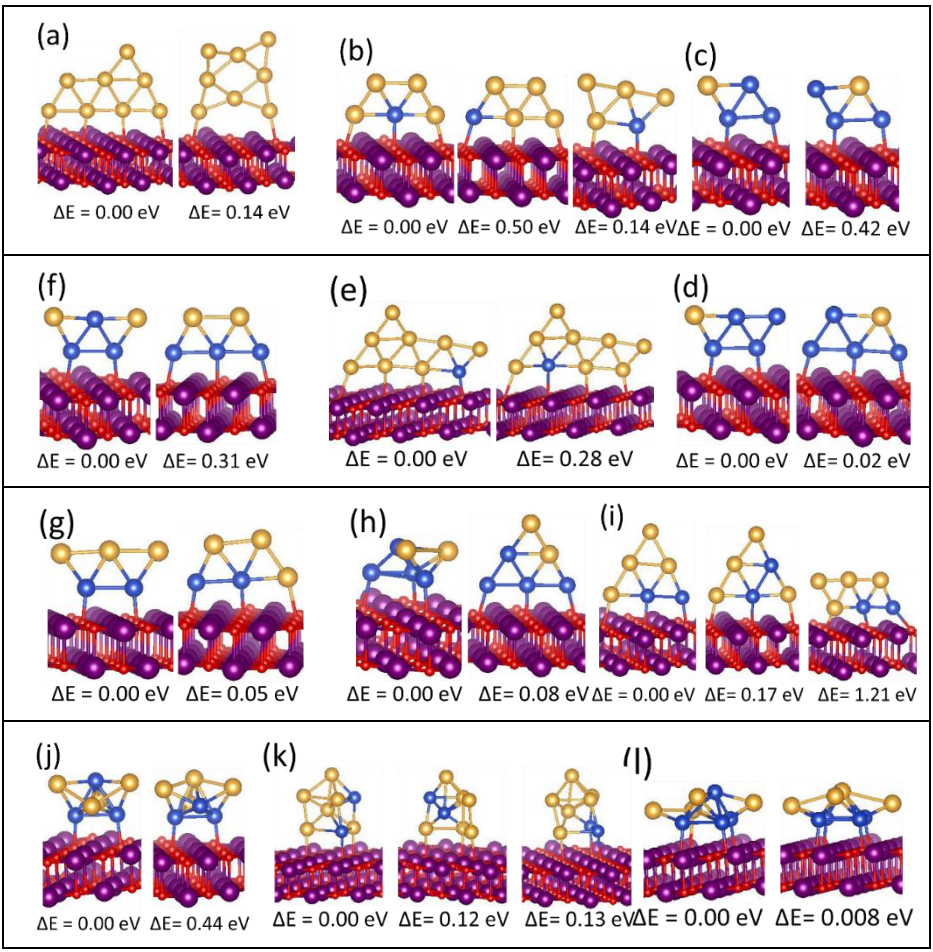

Fig. 8: Putative global minimum (left) versus local minima (right) for the MgO(100)-supported clusters of (a) Au_8, (b) Au_4Cu_1, (c) Au_1Cu_3, (d) Au_1Cu_4, (e) Au_8Cu_1, (f) Au_2Cu_3, (g) Au_3Cu_2, (h) Au_2Cu_4, (i) Au_4Cu_2, (j) Au_4Cu_3, (k) Au_6Cu_2, and (l) Au_4Cu_4.

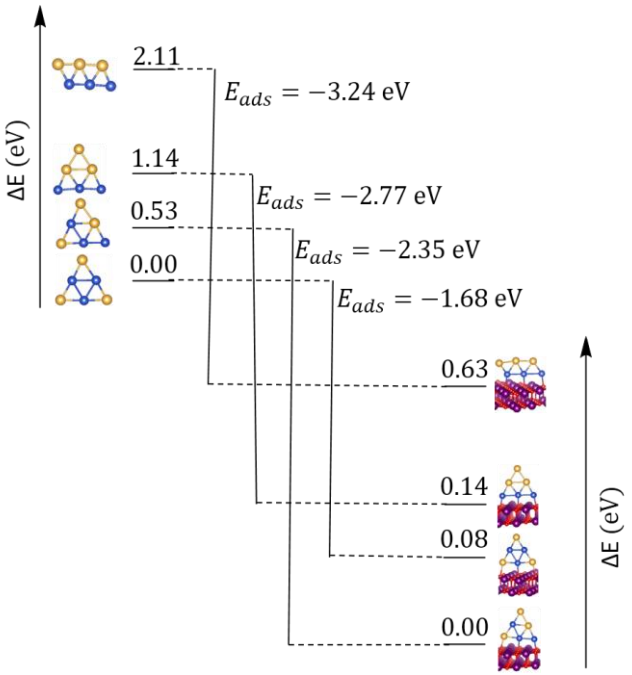

Fig. 9: Potential energy profile, relative energies and adsorption energies, of some alternative isomers for free and supported Au_3Cu_3 clusters, compared with their free and supported GM.

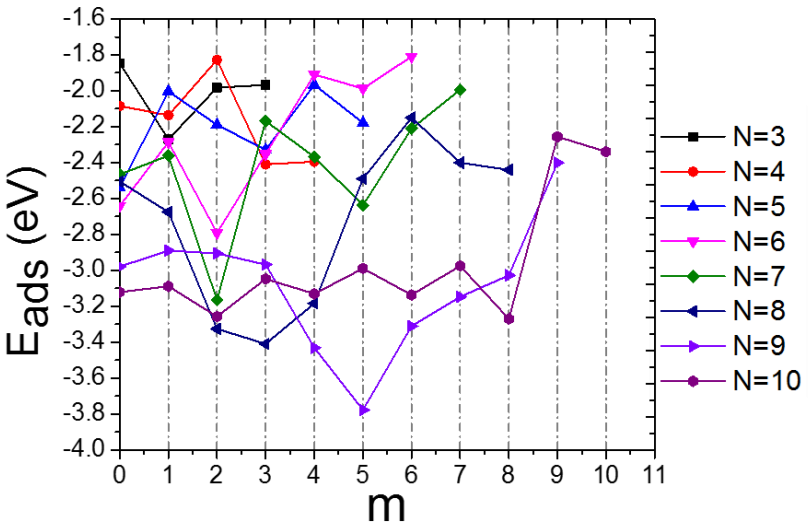

Fig. 10: Adsorption energies E_{ads} plotted against the number of Au atoms, m, for MgO(100)-supported Au_mCu_{N-m} clusters (N=3-10).

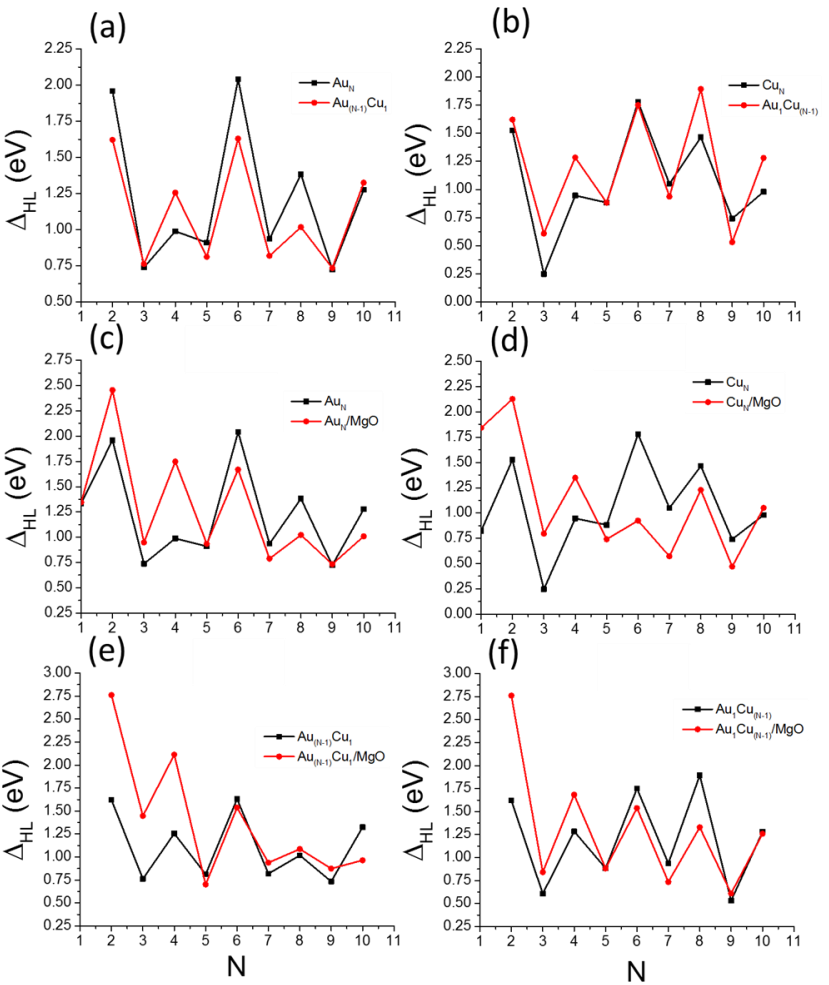

Fig. 11: HOMO-LUMO energy gaps plotted against the total number of atoms, N, for free and MgO(100)-supported pure and mono-doped clusters (N=2-10).

Associated Content

Supporting Information is attached.

Acknowledgment

H. A. Hussein is grateful to the University of Kufa and the Ministry of Higher Education and Scientific Research (Iraq) for the award of a PhD scholarship. Calculations were performed on: the University of Birmingham's BlueBEAR high-performance computer (see http://www.bear.bham.ac.uk/bluebear); ATHENA at HPC Midlands Plus, which is funded by the EPSRC through grant (EP/P020232); and ARCHER, the UK National Supercomputing Service (see http://www.archer.ac.uk) via membership of the UK's HPC Materials Chemistry Consortium, which is funded by EPSRC (EP/L000202), and "TOUCAN: Towards an Understanding of Catalysis on Nanoalloys" membership, which is funded by EPSRC under Critical Mass Grant (EP/J010804/1). H. A. Hussein thanks John Hey for useful discussions and technical advice.

References

[1] C. T. Campbell, Ultrathin metal films and particles on oxide surfaces: structural, electronic and chemisorptive properties, *Surf. Sci. Rep*, 1997, **27**, 4630.

[2] H. Grönbeck and P. Broqvist, Pt and Pt_2on MgO(100) and BaO(100): Structure, bonding, and chemical properties, *J. Chem. Phys.*, 2003, **119**, 3896–3904.

[3] R. I. Razouk and R. S. Mikhail, Surface properties of magnesium oxide, *J. Phys. Chem.*, 1957, **61**, 886–891.

[4] N. T. K. Thanh, N. Maclean and S. Mahiddine, Mechanisms of nucleation and growth of nanoparticles in solution, *Chem. Rev.*, 2014, **114**, 7610–7630.

[5] G. Barcaro and A. Fortunelli, Structure and diffusion of small Ag and Au clusters on the regular MgO (100) surface, *New J. Phys.*, 2007, **9**, 22.

[6] C. R. Henry, Surface studies of supported model catalysts, *Surf. Sci. Rep.*, 1998, **31**, 231–325.

[7] H. J. Freund, Clusters and islands on oxides: From catalysis via electronics and magnetism to optics, *Surf. Sci.*, 2002, **500**, 271–299.

[8] L. Ma, K. Laasonen and J. Akola, Catalytic Activity of AuCu Clusters on MgO(100): Effect of Alloy Composition for CO Oxidation, *J. Phys. Chem. C*, 2017, **121**, 10876–10886.

[9] G. Barcaro and A. Fortunelli, A study of bimetallic Cu-Ag, Au-Ag and Pd-Ag clusters adsorbed on a double-vacancy-defected MgO(100) terrace, *Faraday Discuss.*, 2008, **138**, 37–47.

[10] I. Yudanov, G. Pacchioni, K. Neyman and N. Rösch, Systematic Density Functional Study of the Adsorption of Transition Metal Atoms on the MgO(001) Surface, *J. Phys. Chem. B*, 1997, **101**, 2786–2792.

[11] A. V. Matveev, K. M. Neyman, I. V. Yudanov and N. Rösch, Adsorption of transition metal atoms on oxygen vacancies and regular sites of the MgO(001) surface, *Surf. Sci.*, 1999, **426**, 123–139.

[12] N. Lopez, F. Illas, N. Rösch and G. Pacchioni, Adhesion energy of Cu atoms on the MgO(001) surface, *J. Chem. Phys.*, 1999, **110**, 4873–4879.

[13] G. Barcaro and A. Fortunelli, The Interaction of Coinage Metal Clusters with the MgO(100) Surface, *J. Chem. Theory Comput.*, 2005, **1**, 972–985.

[14] P. Ferrari, H. A. Hussein, C. J. Heard, J. Vanbuel, R. L. Johnston, P. Lievens and E. Janssens, Effect of palladium doping on the stability and fragmentation patterns

of cationic gold clusters, *Phys. Rev. A*, 2018, **97**, 1–10.

[15] V. Kaydashev, P. Ferrari, C. Heard, E. Janssens, R. L. Johnston and P. Lievens, Optical Absorption of Small Palladium-Doped Gold Clusters, *Part. Part. Syst. Charact.*, 2016, **33**, 364–372.

[16] H. Häkkinen, S. Abbet, A. Sanchez, U. Heiz and U. Landman, Structural, electronic, and impurity-doping effects in nanoscale chemistry: Supported gold nanoclusters, *Angew. Chemie - Int. Ed.*, 2003, **42**, 1297–1300.

[17] B. Kiran, X. Li, H. J. Zhai, L. F. Cui and L. S. Wang, [SiAu4]: Aurosilane, *Angew. Chemie - Int. Ed.*, 2004, **43**, 2125–2129.

[18] R. Pal, L. M. Wang, W. Huang, L. S. Wang and X. C. Zeng, Structural evolution of doped gold clusters: MAu_x^- (M = Si, Ge, Sn; x = 5-8), *J. Am. Chem. Soc.*, 2009, **131**, 3396–3404.

[19] S. Nigam and C. Majumder, M atom (M= Cu, Ag and Au) interaction with Ag and Au substrates: A first-principles study using cluster and slab models, *J. Phys. Condens. Matter*, 2010, **22**, 435001.

[20] P. Pyykkö and N. Runeberg, Icosahedral WAu_{12}: A Predicted Closed-Shell Species, Stabilized by Aurophilic Attraction and Relativity and in Accord with the 18-Electron Rule, *Angew. Chem. Int. Edn*, 2002, **41**, 2174–2176.

[21] H. Tanaka, S. Neukermans, E. Janssens, R. E. Silverans and P. Lievens, Density functional study on structure and stability of bimetallic Au_NZn (N≤6) clusters and their cations, *J. Chem. Phys.*, 2003, **119**, 7115–7123.

[22] Y. Gao, S. Bulusu and X. C. Zeng, Gold-caged metal clusters with large HOMO-LUMO gap and high electron affinity, *J. Am. Chem. Soc.*, 2005, **127**, 15680–15681.

[23] J. Monzó, Y. Malewski, R. Kortlever, F. J. Vidal-Iglesias, J. Solla-Gullón, M. T. M. Koper and P. Rodriguez, Enhanced electrocatalytic activity of Au@Cu core@shell nanoparticles towards CO_2 reduction, *J. Mater. Chem. A*, 2015, **3**, 23690–23698.

[24] D. T. Whipple and P. J. A. Kenis, Prospects of CO_2 utilization via direct heterogeneous electrochemical reduction, *J. Phys. Chem. Lett.*, 2010, **1**, 3451–3458.

[25] L. Delannoy, G. Thrimurthulu, P. S. Reddy, C. Méthivier, J. Nelayah, B. M. Reddy, C. Ricolleau and C. Louis, Selective hydrogenation of butadiene over TiO_2 supported copper, gold and gold-copper catalysts prepared by deposition-precipitation, *Phys. Chem. Chem. Phys.*, 2014, **16**, 26514–26527.

[26] Z. Xu, E. Lai, S. H. Yang and K. Hamad-Schifferli, Compositional dependence of the stability of AuCu alloy nanoparticles, *Chem. Commun.*, 2012, **48**, 5626–5628.

[27] A. A. Peterson, F. Abild-Pedersen, F. Studt, J. Rossmeisl and J. K. Nørskov, How copper catalyzes the electroreduction of carbon dioxide into hydrocarbon fuels, *Energy Environ. Sci.*, 2010, **3**, 1311–1315.

[28] Y. Hori, in *Modern Aspects of Electrochemistry*, eds. G. Vayenas, R. E. White and M. E. Gamboa-Aldeco, Springer, New York, 2008, pp. 89–189.

[29] J. J. Kim and J. K. W. Frese, Reduction of carbon dioxide and carbon monoxide to methane on copper foil electrodes, *J. Electroanal. Chem.*, 1988, **245**, 223–244.

[30] S. Pace, T. Van Hoof, M. Hou, C. Buess-Herman and F. Reniers, Surface composition of CuAu single crystal electrodes determined by a coupled UHV-electrochemical approach and a Monte-Carlo simulation, *Surf. Interface Anal.*, 2004, **36**, 1078–1082.

[31] L. Wang and J. C. Yang, Enhanced nucleation and decreased growth rates of Cu_2O in $Cu_{0.5}Au_{0.5}$ (001) thin films during in situ oxidation, *J. Mater. Res.*, 2005, **20**, 1902–1909.

[32] D. P. Whittle, D. J. Evans, D. B. Scully and G. C. Wood, Compositional changes in the underlying alloy during the protective oxidation of alloys, *Acta Met.*, 1967, **15**,

1421.

[33] S. Lysgaard, J. S. G. Mýrdal, H. A. Hansen and T. Vegge, A DFT-based genetic algorithm search for AuCu nanoalloy electrocatalysts for CO_2 reduction, *Phys. Chem. Chem. Phys.,* 2015,**17**, 28270-28276.

[34] C. Kittel, *Introduction to solid state physics*, Wiley, New York, 7th edn., 1996.

[35] C. J. Heard and R. L. Johnston, A density functional global optimisation study of neutral 8-atom Cu-Ag and Cu-Au clusters, *Eur. Phys. J. D*, 2013, **67**, 34.

[36] A. S. Bandarenka, A. S. Varela, M. Karamad, F. Calle-Vallejo, L. Bech, F. J. Perez-Alonso, J. Rossmeisl, I. E. L. Stephens and I. Chorkendorff, Design of an active site towards optimal electrocatalysis: Overlayers, surface alloys and near-surface alloys of Cu/Pt (111), *Angew. Chemie - Int. Ed.*, 2012, **51**, 11845–11848.

[37] R. Cai, P. R. Ellis, J. Yin, J. Liu, C. M. Brown, R. Griffin, G. Chang, D. Yang, J. Ren, K. Cooke, P. T. Bishop, W. Theis and R. E. Palmer, Performance of Preformed Au/Cu Nanoclusters Deposited on MgO Powders in the Catalytic Reduction of 4-Nitrophenol in Solution, *Small*, 2018, **14**, 1703734.

[38] S. Back, J. H. Kim, Y. T. Kim and Y. Jung, Bifunctional interface of Au and Cu for improved CO_2 electroreduction, *ACS Appl. Mater. Interfaces*, 2016, **8**, 23022–23027.

[39] C. L. Bracey, P. R. Ellis and G. J. Hutchings, Application of copper–gold alloys in catalysis: current status and future perspectives, *Chem. Soc. Rev.*, 2009, **38**, 2231–2243.

[40] X. Liu, A. Wang, L. Li, T. Zhang, C. Y. Mou and J. F. Lee, Structural changes of Au-Cu bimetallic catalysts in CO oxidation: In situ XRD, EPR, XANES, and FT-IR characterizations, *J. Catal.*, 2011, **278**, 288–296.

[41] J. C. Bauer, D. Mullins, M. Li, Z. Wu, E. A. Payzant, S. H. Overbury and S. Dai, Synthesis of silica supported AuCu nanoparticle catalysts and the effects of pretreatment conditions for the CO oxidation reaction, *Phys. Chem. Chem. Phys.*, 2011, **13**, 2571–2581.

[42] F. Yin, Z. W. Wang and R. E. Palmer, Controlled formation of mass-selected Cu-Au core-shell cluster beams, *J. Am. Chem. Soc.*, 2011, **133**, 10325–10327.

[43] B. Pauwels, G. Van Tendeloo, E. Zhurkin, M. Hou, G. Verschoren, L. T. Kuhn, W. Bouwen and P. Lievens, Transmission electron microscopy and Monte Carlo simulations of ordering in Au-Cu clusters produced in a laser vaporization source, *Phys. Rev. B*, 2001, **63**, 165406.

[44] T. J. Toai, G. Rossi and R. Ferrando, Global optimisation and growth simulation of AuCu clusters, *Faraday Discuss.*, 2008, **138**, 49–58.

[45] E. Ringe, R. P. Van Duyne and L. D. Marks, Wulff construction for alloy nanoparticles, *Nano Lett.*, 2011, **11**, 3399–3403.

[46] F. Yin, Z. W. Wang and R. E. Palmer, Ageing of mass-selected Cu/Au and Au/Cu core/shell clusters probed with atomic resolution, *J. Exp. Nanosci.*, 2012, **7**, 703–710.

[47] Z. P. Liu, P. Hu and A. Alavi, Catalytic role of gold in gold-based catalysts: A density functional theory study on the CO oxidation on gold, *J. Am. Chem. Soc.*, 2002, **124**, 14770–14779.

[48] A. Sandoval, C. Louis and R. Zanella, Improved activity and stability in CO oxidation of bimetallic Au-Cu/TiO_2 catalysts prepared by deposition-precipitation with urea, *Appl. Catal. B Environ.*, 2013, **140–141**, 363–377.

[49] T. S. Mozer, D. A. Dziuba, C. T. P. Vieira and F. B. Passos, The effect of copper on the selective carbon monoxide oxidation over alumina supported gold catalysts, *J. Power Sources*, 2009, **187**, 209–215.

[50] L. Ma, M. Melander, T. Weckman, K. Laasonen and J. Akola, CO Oxidation on the

$Au_{15}Cu_{15}$ Cluster and the Role of Vacancies in the MgO(100) Support, *J. Phys. Chem. C*, 2016, **120**, 26747−26758.

[51] U. Heiz, A. Sanchez, S. Abbet and W. D. Schneider, Catalytic oxidation of carbon monoxide on monodispersed platinum clusters: Each atom counts, *J. Am. Chem. Soc.*, 1999, **121**, 3214–3217.

[52] U. Landman, Materials by numbers: Computations as tools of discovery, *Proc. Natl. Acad. Sci.*, 2005, **102**, 6671–6678.

[53] D. T. Tran, I. P. Jones, J. A. Preece, R. L. Johnston and C. R. Van Den Brom, TEM characterization of chemically synthesized copper-gold nanoparticles, *J. Nanoparticle Res.*, 2011, **13**, 4229–4237.

[54] N. T. Wilson and R. L. Johnston, A theoretical study of atom ordering in copper-gold nanoalloy clusters, *J. Mater. Chem.*, 2002, **12**, 2913–2922.

[55] M. Cerbelaud, G. Barcaro, A. Fortunelli and R. Ferrando, Theoretical study of AuCu nanoalloys adsorbed on MgO(001), *Surf. Sci.*, 2012, **606**, 938–944.

[56] H. A. Hussein and R. L.Johnston, in *Frontiers of Nanoscience: Computational Modelling of Nanoparticles*, eds. S. T. Bromley and S. M. Woodley, Elsevier, Amsterdam, 2019, pp. 145–169.

[57] R. L. Johnston, Evolving better nanoparticles: Genetic algorithms for optimising cluster geometries, *Dalt. Trans.*, 2003, 4193–4207.

[58] C. J. Heard, A. Shayeghi, R. Schäfer, and R. L. Johnston, Charge and Compositional Effects on the 2D–3D Transition in Octameric AgAu Clusters, *Z. Phys. Chem.*, 2016, **230**, 955–975.

[59] J. A. Vargas, F. Buendía and M. R. Beltrán, New Au_N (N = 27-30) Lowest Energy Clusters Obtained by Means of an Improved DFT-Genetic Algorithm Methodology, *J. Phys. Chem. C*, 2017, **121**, 10982–10991.

[60] J. Davis, A. Shayeghi, S. L. Horswell and R. L. Johnston, The Birmingham Parallel Genetic Algorithm and its application to the direct DFT global optimisation of Ir_N (N = 10 − 20) clusters., *Nanoscale*, 2015, **7**, 14032–14038.

[61] A. Shayeghi, D. Götz, J. B. A. Davis, R. Schäfer and R. L. Johnston, Pool-BCGA: a parallelised generation-free genetic algorithm for the ab initio global optimisation of nanoalloy clusters, *Phys. Chem. Chem. Phys.*, 2015, **17**, 2104–2112.

[62] B. Bandow and B. Hartke, Larger water clusters with edges and corners on their way to ice: Structural trends elucidated with an improved parallel evolutionary algorithm, *J. Phys. Chem. A*, 2006, **110**, 5809–5822.

[63] D. Deaven and K. Ho, Molecular Geometry Optimization with a Genetic Algorithm, *Phys. Rev. Lett.*, 1995, **75**, 288–291.

[64] G. Kresse and J. Hafner, Ab initio molecular dynamics for liquid metals, *Phys. Rev. B*, 1993, **47**, 558–561.

[65] J. Perdew, K. Burke and Y. Wang, Generalized gradient approximation for the exchange-correlation hole of a many-electron system, *Phys. Rev. B*, 1996, **54**, 16533–16539.

[66] G. Kresse, From ultrasoft pseudopotentials to the projector augmented-wave method, *Phys. Rev. B*, 1999, **59**, 1758–1775.

[67] M. Methfessel and A. T. Paxton, High-precision sampling for Brillouin-zone integration in metals, *Phys. Rev. B*, 1989, **40**, 3616–3621.

[68] T. Koopmans, Über die Zuordnung von Wellenfunktionen und Eigenwerten zu den Einzelnen Elektronen Eines Atoms, *Physica*, 1933, **1**, 104.

[69] B. Assadollahzadeh and P. Schwerdtfeger, A systematic search for minimum structures of small gold clusters Au_n (n=2-20) and their electronic properties, *J. Chem. Phys.*, 2009, **131**, 064306.

[70] H. A. Hussein, J. B. A. Davis and R. L. Johnston, DFT global optimisation of gas-

phase and MgO-supported sub-nanometre AuPd clusters, *Phys. Chem. Chem. Phys.*, 2016, **18**, 26133–26143.

[71] G. Zanti and D. Peeters, DFT study of bimetallic palladium-gold clusters Pd_nAu_m of low nuclearities (n + m ≤ 14), *J. Phys. Chem. A*, 2010, **114**, 10345–10356.

[72] L. Xiao, B. Tollberg, X. Hu and L. Wang, Structural study of gold clusters, *J. Chem. Phys.*, 2006, **124**, 114309.

[73] V. Bonačić-Koutecký, J. Burda, R. Mitrić, M. Ge, G. Zampella and P. Fantucci, Density functional study of structural and electronic properties of bimetallic silver–gold clusters: Comparison with pure gold and silver clusters, *J. Chem. Phys.*, 2002, **117**, 3120.

[74] J. Wang, G. Wang and J. Zhao, Density functional study of Au_n (n = 2− 20) clusters: lowest-energy structures and electronic properties, *Phys. Rev. B*, 2002, **66**, 35418.

[75] P. Schwerdtfeger and M. Lein, in *Gold Chemistry: Applications and Future Directions in the Life Sciences*, ed. F. Mohr, Wiley, New York, 2009, p. 183.

[76] C. G. Li, J. Zhang, Y. Q. Yuan, Y. N. Tang, B. Z. Ren and W. G. Chen, Geometries, stabilities and electronic properties of copper and selenium doped copper clusters: Density functional theory study, *Phys. E Low-Dimensional Syst. Nanostructures*, 2017, **86**, 303–310.

[77] P. Jaque and A. Toro-Labbé, Characterization of copper clusters through the use of density functional theory reactivity descriptors, *J. Chem. Phys.*, 2002, **117**, 3208–3218.

[78] G. Guzmán-Ramírez, F. Aguilera-Granja and J. Robles, DFT and GEGA genetic algorithm optimized structures of Cu_n^v (v=±1,0,2; N=3-13) clusters, *Eur. Phys. J. D*, 2010, **57**, 49–60.

[79] R. Passalacqua, S. Parathoner, G. Centi, A. Halder, E. C. Tyo, B. Yang, S. Seifert and S. Vajda, Electrochemical behaviour of naked sub-nanometre sized copper clusters and effect of CO_2, *Catal. Sci. Technol.*, 2016, **6**, 6977–6985.

[80] S. Huseyinova, J. Blanco, F. G. Requejo, J. M. Ramallo-López, M. C. Blanco, D. Buceta and M. A. López-Quintela, Synthesis of Highly Stable Surfactant-free Cu_5 Clusters in Water, *J. Phys. Chem. C*, 2016, **120**, 15902–15908.

[81] a) S. Darby, T. V. Mortimer-Jones, R. L. Johnston and C. Roberts, Theoretical study of Cu-Au nanoalloy clusters using a genetic algorithm, *J. Chem. Phys.*, 2002, **116**, 1536–1550. b) J- Goh, J. Akola, and R. Ferrando, Geometric Structure and Chemical Ordering of Large AuCu Clusters: A Computational Study, *J. Phys. Chem. C*, 2017, **121**, 10809–10816.

[82] X. Wu, W. Cai and X. Shao, Optimization of Bimetallic Cu–Au and Ag–Au Clusters by Using a Modified Adaptive Immune Optimization Algorithm, *J. Comput. Chem.*, 2009, **30**, 1992–2000.

[83] I. L. Garzón, K. Michaelian, M. R. Beltrán, A. Posada-Amarillas, P. Ordejón, E. Artacho, D. Sánchez-Portal and J. M. Soler, Lowest energy structures of gold nanoclusters, *Phys. Rev. Lett.*, 1998, **81**, 1600–1603.

[84] A. Rapallo, G. Rossi, R. Ferrando, A. Fortunelli, B. C. Curley, L. D. Lloyd, G. M. Tarbuck and R. L. Johnston, Global optimization of bimetallic cluster structures. I. Size-mismatched Ag-Cu, Ag-Ni, and Au-Cu systems, *J. Chem. Phys.*, 2005, **122**, 194308.

[85] R. A. Lordeiro, F. F. Guimarães, J. C. Belchior and R. L. Johnston, Determination of main structural compositions of nanoalloy clusters of Cu_xAu_y (x + y ≤ 30) using a genetic algorithm approach, *Int. J. Quantum Chem.*, 2003, **95**, 112–125.

[86] a) K. M. Neyman, C. Inntam, V. A. Nasluzov, R. Kosarev and N. Rösch, Adsorption of d-metal atoms on the regular MgO(001) surface: Density functional study of cluster models embedded in an elastic polarizable environment, *Appl. Phys. A*,

2004, **78**, 823-828. b) G. Barcaro and A. Fortunelli, The interaction of coinage metal clusters with the MgO(100) surface, *J. Chem. Theory Comput.*, 2005, **1**, 972–985.

[87] F. Buend, M. R. Beltr and R. L. Johnston, Systematic Comparative Study of Au_nRh_{N-n} (N = 4-6) Clusters in Gas Phase Versus Deposited on (100) MgO, *Phys. Chem. Chem. Phys.*, 2015, **18**, 22122.

[88] J. B. A. Davis, S. L. Horswell and R. L. Johnston, Application of a Parallel Genetic Algorithm to the Global Optimization of Gas-Phase and Supported Gold–Iridium Sub-Nanoalloys, *J. Phys. Chem. C*, 2016, **120**, 3759–3765.

[89] K. J. Taylor, C. L. P. Hall, O. Cheshnovsky, R. E. Smalley, K. J. Taylor, C. L. Pettiette-hall, O. Cheshnovsky and R. E. Smalley, Ultraviolet photoelectron spectra of coinage metal clusters Ultraviolet photoelectron spectra of coinage metal clusters, *J. Chem. Phys.*, 1992, **96**, 3319.

[90] T. H. Lee and K. M. Ervin, Reactions of copper group cluster anions with oxygen and carbon monoxide, *J. Phys. Chem.*, 1994, **98**, 10023–10031.

[91] D. Stolcic, M. Fischer, G. Gantefo, Y. D. Kim, Q. Sun and P. Jena, Direct Observation of Key Reaction Intermediates on Gold Clusters, *J. Am. Chem. Soc.*, 2003, **125**, 2848–2849.

[92] D. Chan, R. Dietsche, G. Ganteför and Y. Dok, Chemical properties of size-selected Au clusters treated under ambient conditions, *Chem. Phys. Lett.*, 2008, **457**, 391–395.

[93] H. A. Hussein, I. Demiroglu and R. L. Johnston, Application of a parallel genetic algorithm to the global optimization of medium-sized Au-Pd sub-nanometre clusters, *Eur. Phys. J. B*, 2018, **91**, 34.

[94] I. Demiroglu, K. Yao, H. A. Hussein and R. L. Johnston, DFT Global Optimization of Gas-Phase Subnanometer Ru−Pt Clusters, *J. Phys. Chem. C Artic. ASAP*, 2017, **121**, 10773–10780.

[95] X. Teng, Q. Wang, P. Liu, W. Han, A. I. Frenkel, W. Wen, N. Marinkovic, J. C. Hanson and J. A. Rodriguez, Formation of Pd/Au Nanostructures from Pd Nanowires via Galvanic Replacement Reaction, *J. Am. Chem. Soc.*, 2008, **130**, 1093–1101.

[96] M. Daniel and D. Astruc, Gold Nanoparticles: Assembly, Supramolecular Chemistry, Quantum-Size-Related Properties, and Applications toward Biology, Catalysis, and Nanotechnology, *Chem. Rev.*, 2004, **104**, 239–346.

[97] P. Ranjan, S. Venigalla and A. Kumar, A theoretical study of bi-metallic Ag_mAu_n; (m+n=2-8) nano alloy clusters in terms of DFT based descriptors, *New Front. Chem.*, 2014, **23**, 111–122.

[98] R. G. Pearson, Recent advances in the concept of hard and soft acids and bases, *J. Chem. Educ.*, 1987, **64**, 561.

[99] R. Pearson, Chemical hardness and density functional theory, *J. Chem.. Sci.*, 2005, **117**, 369–377.

[100] R. G. Parr and P. K. Chattaraj, Principle of Maximum Hardness, *J. Am. Chem. Soc.*, 1991, **113**, 1854–1855.

[101] R. G. Parr and R. G. Pearson, Absolute Hardness: Companion Parameter to Absolute Electronegativity, *J. Am. Chem. Soc.*, 1983, **105**, 7512–7516.

[102] G. Guzmán-Ramírez, F. Aguilera-Granja and J. Robles, DFT study of the fragmentation channels and electronic properties of Cu_n^v (v= ±1,0,2; N=3-13) clusters, *Eur. Phys. J. D*, 2010, **57**, 335–342.

[103] X. Hai, J. Tahir-Kheli and W. A. Goddard, Accurate band gaps for semiconductors from density functional theory, *J. Phys. Chem. Lett.*, 2011, **2**, 212–217.